Complex I assembly into supercomplexes determines differential mitochondrial ROS production in neurons and astrocytes

Irene Lopez-Fabuel[a], Juliette Le Douce[b], Angela Logan[c], Andrew M. James[c], Gilles Bonvento[b], Michael P. Murphy[c], Angeles Almeida[d], and Juan P. Bolaños[a,1]

[a]Institute of Functional Biology and Genomics, University of Salamanca–Consejo Superior de Investigaciones Cientificas, 37007 Salamanca, Spain; [b]Commissariat à l'Energie Atomique et aux Energies Alternatives, Département des Sciences du Vivant, Institut d'Imagerie Biomédicale, Molecular Imaging Center, CNRS UMR 9199, Université Paris-Sud, Université Paris-Saclay, F-92260 Fontenay-aux-Roses, France; [c]Medical Research Council Mitochondrial Biology Unit, Cambridge Biomedical Campus, Cambridge CB2 0XY, United Kingdom; and [d]Institute of Biomedical Research of Salamanca, University Hospital of Salamanca, 37007 Salamanca, Spain

Edited by Rafael Radi, Universidad de la Republica, Montevideo, Uruguay, and approved September 23, 2016 (received for review August 18, 2016)

Neurons depend on oxidative phosphorylation for energy generation, whereas astrocytes do not, a distinctive feature that is essential for neurotransmission and neuronal survival. However, any link between these metabolic differences and the structural organization of the mitochondrial respiratory chain is unknown. Here, we investigated this issue and found that, in neurons, mitochondrial complex I is predominantly assembled into supercomplexes, whereas in astrocytes the abundance of free complex I is higher. The presence of free complex I in astrocytes correlates with the severalfold higher reactive oxygen species (ROS) production by astrocytes compared with neurons. Using a complexomics approach, we found that the complex I subunit NDUFS1 was more abundant in neurons than in astrocytes. Interestingly, NDUFS1 knockdown in neurons decreased the association of complex I into supercomplexes, leading to impaired oxygen consumption and increased mitochondrial ROS. Conversely, overexpression of NDUFS1 in astrocytes promoted complex I incorporation into supercomplexes, decreasing ROS. Thus, complex I assembly into supercomplexes regulates ROS production and may contribute to the bioenergetic differences between neurons and astrocytes.

redox | brain | bioenergetics | lactate | glycolysis

The brain is a metabolically demanding organ (1) that requires tight cooperation between neurons and astrocytes (2). Astrocytes provide crucial metabolic and structural support (3, 4) and are key players in neurotransmission (5–7) and behavior (8). The status of many major redox couples in the brain is also regulated by astrocytes (9), through their high content of antioxidant compounds and enzymes (10) and by the constitutive stabilization of the master antioxidant transcriptional activator, nuclear factor erythroid 2-related factor 2 (Nrf2) (11). Thus, astrocytes are equipped to protect themselves when exposed to excess reactive oxygen species (ROS) (12) and reactive nitrogen species (13, 14). Moreover, astrocytes also provide nearby neurons with protective antioxidant precursors through a cell-signaling mechanism involving glutamate receptor activation by neurotransmission (11, 15, 16). The tight coupling between astrocytes and neurons therefore helps in energy and redox metabolism during normal brain function.

Intriguingly, the ATP used by neurons is supplied by oxidative phosphorylation, whereas most energy needs of astrocytes are met by glycolysis (17). In fact, the survival of neurons requires oxidative phosphorylation (18, 19). The different energy metabolisms of the two cell types are closely coupled, with astrocytes releasing the glycolytic end product, lactate, which is used by neighboring neurons to drive oxidative phosphorylation (20–22). As the molecular mechanisms underlying the markedly different modes of ATP production in the two cell types are not understood, we investigated whether the organization of the mitochondrial respiratory chain in brain cells could contribute. Here, we report that the extent of supercomplex formation by the mitochondrial respiratory chain is quite different in neurons and astrocytes and that these structural differences regulate different rates of mitochondrial ROS production and respiration.

Results

More Complex I Is Free in Astrocytes than in Neurons, Affecting Mitochondrial Function and ROS Production. Mitochondrial complexes can organize into supercomplexes in a process that has been claimed to regulate electron transfer efficiency (23). Therefore, we assessed whether the structural organization of the mitochondrial respiratory chain differed between neurons and astrocytes. To do this, digitonin-solubilized mitochondria (24) from primary cultures of C57BL/6 mouse neurons and astrocytes were analyzed by blue native gel electrophoresis (BNGE). Complex I occurred both on its own and also bound with complex III, notably in a I+III_2 supercomplex and, to a lesser extent, in a I_2+III_2 supercomplex (Fig. 1*A*) (25). The composition of these supercomplexes was confirmed by electrotransfer of the proteins to nitrocellulose followed by immunoblotting against either a complex I subunit (NADH:ubiquinone oxidoreductase subunit B8, NDUFB8) or a complex III subunit (ubiquinol-cytochrome C reductase core protein III, UQCRC2) (Fig. 1*A*). Interestingly, we observed a significant difference between astrocytes and neurons in the proportion of complex I that was free relative to that which was part of a supercomplex. The ratio of free

Significance

Neurons depend on oxidative phosphorylation for survival, whereas astrocytes do not. Mitochondrial respiratory chain (MRC) complexes can be organized in higher structures called supercomplexes, which dictate MRC electron flux and energy efficiency. Whether the specific metabolic shapes of neurons and astrocytes are determined by the specific organization of MRC complexes is unknown. Here, we found that, in astrocytes, most complex I is free, resulting in poor mitochondrial respiration but high reactive oxygen species (ROS) production. In contrast, neurons show complex I to be mostly embedded into supercomplexes, thus resulting in high mitochondrial respiration and low ROS production. Thus, MRC organization dictates different bioenergetics preferences of neurons and astrocytes impacting on ROS production, possibly playing a role in neurodegenerative diseases.

Author contributions: J.P.B. designed research; I.L.-F., J.L.D., A.L., A.M.J., G.B., M.P.M., and A.A. performed research; I.L.-F., A.L., M.P.M., A.A., and J.P.B. analyzed data; and J.P.B. wrote the paper.

The authors declare no conflict of interest.

This article is a PNAS Direct Submission.

Freely available online through the PNAS open access option.

[1]To whom correspondence should be addressed. Email: jbolanos@usal.es.

This article contains supporting information online at www.pnas.org/lookup/suppl/doi:10.1073/pnas.1613701113/-/DCSupplemental.

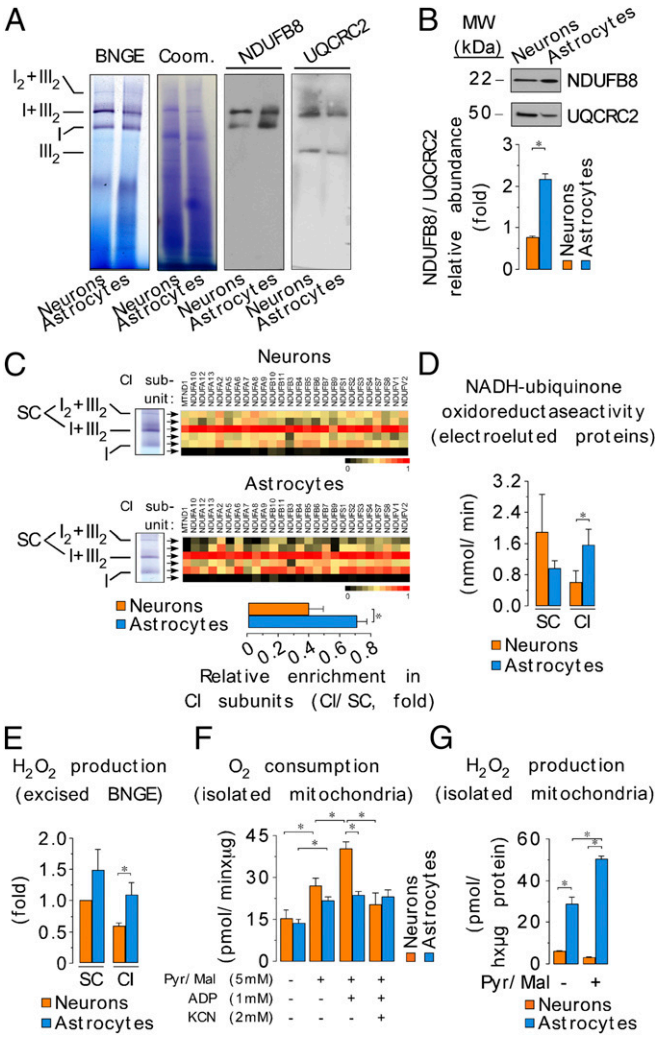

Fig. 1. Different assembly of complex I into supercomplexes between neurons and astrocytes correlates with ROS production and mitochondrial respiration. (*A*) Digitonin-solubilized isolated mitochondria from mouse astrocytes and neurons were subjected to blue native gel electrophoresis (BNGE) followed by in-gel complex I activity assay. Complex I occurs both free and bound with complex III (I+III$_2$ and I$_2$+III$_2$ supercomplexes). Direct electrotransfer of the native proteins to nitrocellulose followed by immunoblotting against NDUFB8 (a complex I subunit) or UQCRC2 (a complex III subunit). (*B*) Western blotting against NDUFB8 and UQCRC2 in whole-cell protein extracts showing the relative abundance of complex I versus complex III in astrocytes and neurons. (*C*) Slices were excised from digitonin-solubilized isolated astrocyte and neuronal mitochondria blue native gels, and the abundances of complex I subunits in free complex I (CI), relative to the abundance of those in I+III$_2$ and I$_2$+III$_2$ supercomplexes (SC), were assessed by complexomics. (*D*) Rotenone-sensitive NADH-ubiquinone oxidoreductase activity of the excised and electroeluted free complex I and complex I-supercomplexes bands from the blue native gel in astrocytes and neurons. Data were not normalized per protein abundance in the eluate, as we aimed to assess the amount of total complex I activity present in each band. (*E*) In-gel H_2O_2 production in the excised SC and CI bands from the BNGE in astrocytes and neurons. H_2O_2 production values were normalized by the NADH dehydrogenase-activity band intensity obtained in the BNGE. (*F*) Pyruvate/malate (5 mM each)-driven mitochondrial oxygen consumption in isolated mitochondria from neurons or astrocytes under state 2 (0 mM ADP) or state 3 (1 mM ADP), either in the absence or in the presence of KCN (2 mM). (*G*) Rate of H_2O_2 production assessed using the AmplexRed assay, in mitochondria isolated from neurons and astrocytes, in the presence and absence of pyruvate/malate (5 mM each). Data are the mean values ± SEM from $n = 3$–4 independent culture preparations (Student's *t* test; ANOVA post hoc Bonferroni). $^*P < 0.05$.

to assembled complex I was higher, whereas the ratio of free to assembled complex III was lower, in astrocytes compared with neurons (Fig. 1*A* and Fig. S1*A*). This pattern of respiratory chain organization was confirmed in freshly isolated neurons and astrocytes (Fig. S1 *B* and *C*) and in cells cultured at 11% O_2, instead of 21% (Fig. S1*D*). The relative abundance of complex I versus complex III in astrocytes was twice that in neurons, as judged by Western blotting of whole-cell extracts (Fig. 1*B*). These data suggest that the relatively low amount of complex III in astrocytes may limit I–III supercomplex formation, and thereby increase the proportion of complex I in astrocytes that is not present in supercomplexes.

To further interrogate the differences in respiratory chain assembly between these two cell types, we next performed proteomic quantitative analyses of complex I subunits by mass spectrometry of gel slices from blue native gels of digitonin-solubilized mitochondria from astrocytes or neurons. As shown in Fig. 1*C*, measurement of complex I subunits showed that their amounts present in free complex I, relative to those present in I+III$_2$ plus I$_2$+III$_2$ supercomplexes, was about twofold greater in astrocytes compared with neurons. This was further assessed by assaying rotenone-sensitive NADH-ubiquinone oxidoreductase activity in proteins electroeluted from blue native gel slices containing the supercomplexes (SC) or free complex I (CI). This showed that the NADH-ubiquinone oxidoreductase activity in the free complex I band was higher in astrocytes than in neurons (Fig. 1*D*). Because complex I catalyzes $O_2^{\bullet-}$ production (26), we next determined ROS in complex I-containing slices excised from the blue native gels, and we found that ROS production from the free complex I band was higher in astrocytes than in neurons (Fig. 1*E*). These results confirm that the ratio of free complex I to that present in supercomplexes is higher in astrocytes than it is in neurons.

Because the organization of respiratory complexes into supercomplexes is reported to affect mitochondrial function and ROS production (24, 25), we next determined O_2 consumption in mitochondria isolated from astrocytes and neurons. State 3 pyruvate/malate-driven (Fig. 1*F*) and succinate-driven (Fig. S1*E*) O_2 consumption in astrocytes was significantly lower than that in neurons. To ascertain whether there were any differences in mitochondrial ROS production between these two cell types, we also determined the rate of H_2O_2 formation in isolated mitochondria. As shown in Fig. 1*G*, mitochondrial ROS production was higher in mitochondria from astrocytes than from neurons, either from endogenous substrates or in the presence of pyruvate/malate. Thus, the presence or absence of complex I in supercomplexes in the respiratory chain in neurons and astrocytes correlates with differences in mitochondrial function and ROS production.

Astrocytes Produce More Mitochondrial ROS than Neurons. To see whether the differences in ROS production by mitochondria isolated from neurons and astrocytes also occurred in intact cells, we determined the rate of H_2O_2 generation by intact neurons and astrocytes in primary cultures from mice and rats. Astrocytes produced H_2O_2 about one order of magnitude faster than neurons, from both rat and mouse and under all culture conditions investigated (Fig. 2*A* and Fig. S2 *A*–*C*). We next assessed mitochondrial ROS production (27) using the mitochondria-targeted probes MitoSox and MitoB (28) in intact cells. The MitoSox fluorescence and the MitoP/MitoB ratio were higher in astrocytes than in neurons (Fig. 2 *B* and *C* and Fig. S2 *D*–*H*), indicating an elevation of mitochondrial ROS in astrocytes compared with neurons under these conditions. Interestingly, the differences in MitoSox fluorescence and in mitochondrial H_2O_2 production, between neurons and astrocytes, were unchanged after $\Delta\psi_m$ disruption with carbonyl cyanide *m*-chlorophenyl hydrazone (CCCP) (Fig. 2 *D* and *E*), suggesting that the difference is not due to differences in $\Delta\psi_m$ affecting probe distribution. Other nonmitochondrial ROS sources, such as xanthine oxidase, NADPH oxidases, and nitric oxide synthase, did not appear to contribute to the high rate of ROS

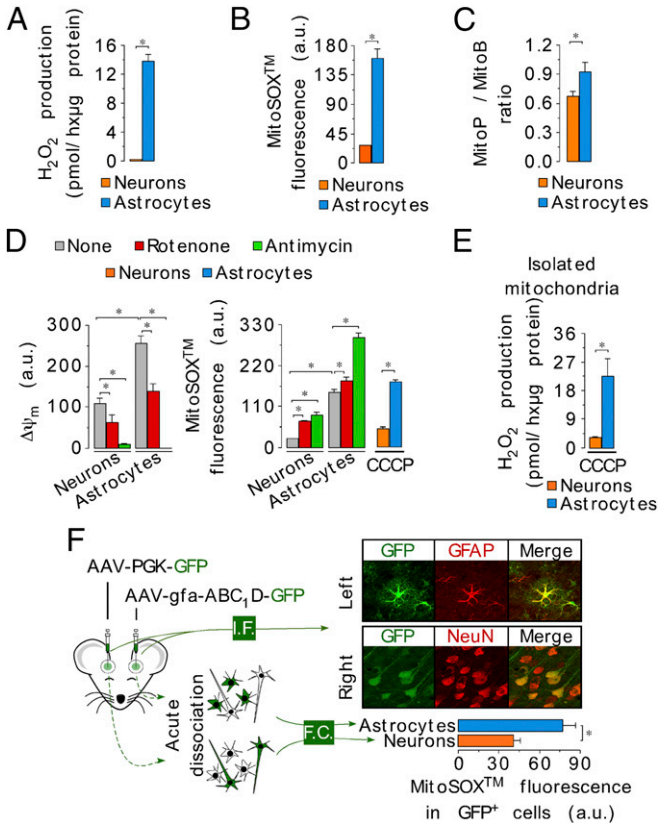

Fig. 2. Higher mitochondrial ROS production in astrocytes than in neurons occurs ex vivo. (*A*) Rates of H_2O_2 production assessed using the AmplexRed assay, in intact C56BL/6 mouse neurons and astrocytes in primary culture. (*B*) Mitochondrial ROS was quantified using the MitoSox assay in the intact cells (C57BL/6) by flow cytometry. (*C*) Mitochondrial ROS levels assessed using MitoB probe. Ratio between MitoP (oxidized form) versus MitoB is normalized per million of cells. (*D*) Mitochondrial membrane potential ($\Delta\psi_m$) (*Left*) and MitoSox fluorescence (*Right*) were determined in basal conditions and after the inhibition of complex I (rotenone) or complex III (antimycin). Rotenone or antimycin was used at 10 μM, each, for 15 min. Furthermore, MitoSox fluorescence was evaluated after cell preincubation with the uncoupler CCCP (10 μM, 15 min). (*E*) Mitochondrial H_2O_2 production after $\Delta\psi_m$ abolishment with the uncoupler CCCP (10 μM). (*F*) Mitochondrial ROS abundance (MitoSox) assessed by flow cytometry (FC) in freshly isolated neurons and astrocytes from adult brain mouse expressing GFP governed either by an astrocyte (gfa-ABC_1D) or a neuronal (PGK) promoter. Cell specificity of promoter-driven GFP expression was validated by immunofluorescence (I.F.) microscopy using astrocyte (GFAP) or neuronal (NeuN) markers. (Magnification: 40×.) Data are the mean values ± SEM from $n = 3$–4 independent culture preparations or $n = 8$ animals (Student's *t* test; ANOVA post hoc Bonferroni). $^*P < 0.05$.

production in astrocytes (Fig. S3 and Table S1). Thus, we conclude that mitochondrial ROS production is greater in astrocytes than in neurons.

We next investigated mitochondrial ROS production in neurons and astrocytes acutely dissociated from the mouse brain. For this, brain cells were isolated from mice previously stereotaxically injected with adenoassociated viruses (AAVs) expressing green fluorescence protein (GFP) under the control of either an astrocyte or a neuronal specific promoter. Cells were then subjected to mitochondrial ROS assessment by flow cytometry analysis using MitoSox. As shown in Fig. 2*F*, the MitoSox fluorescence was higher in astrocyte promoter-driven GFP^+ cells [expressing the astrocyte specific glial-fibrillary acidic protein (GFAP)] than in neuron promoter-driven GFP^+ cells [expressing the neuron-specific neuronal nuclei (NeuN)]. Moreover, freshly isolated mouse brain cells, sorted according to the astrocyte-specific plasma membrane protein integrin β5 (29), showed a similar difference in ROS (Fig. S4 *A* and *B*). Finally, we found that the rate of mitochondrial ROS production was higher in astrocytes than in neurons freshly purified from the mouse brain using magnetic-activated cell sorting (MACS) technology (Fig. S4*C*). Thus, astrocytes produce mitochondrial ROS severalfold faster than neurons.

High ROS Production by Astrocytes Correlates with Deactive Complex I. Given that complex I is a major source of mitochondrial ROS (27), we analyzed the specific activity of complex I in neurons and in astrocytes. As shown in Fig. 3*A*, complex I activity was very similar in both cell types, as were the activities of other respiratory chain complexes (Fig. S5*A*). The complex I inhibitor, rotenone, stimulated mitochondrial ROS production to a great extent in neurons, but only slightly in astrocytes; however, antimycin stimulated mitochondrial ROS production in both cell types (Fig. 2*D* and Fig. S2*H*). The mild effect of rotenone on mitochondrial ROS production in astrocytes was intriguing. Because rotenone stimulates forward (FET) and inhibits the reverse (RET) electron transfer to O_2 at complex I (26, 29), we determined the contribution of RET to ROS production, and we found that RET-mediated ROS is negligible in astrocytes (Fig. S5 *B* and *C*). Because the ubiquinone binding site is inaccessible in deactive complex I (30, 31), rendering it insensitive to rotenone, we hypothesized that there were different proportions of deactive and active complex I in neurons and astrocytes. As shown in Fig. 3*B* (Fig. S5*D*), the proportion of deactive complex

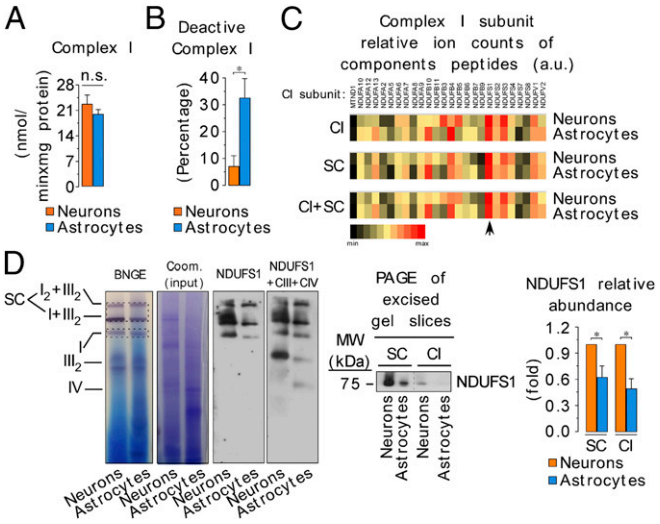

Fig. 3. Astrocytes present a high proportion of deactive complex I, with a reduced abundance of NDUFS1 subunit. (*A*) Mitochondrial complex I (rotenone-sensitive NADH-ubiquinone oxidoreductase) activity, as assessed spectrophotometrically in cell homogenates, in astrocytes and neurons. (*B*) Deactive complex I activity, as assessed by the difference in rotenone-sensitive NADH-ubiquinone oxidoreductase activity obtained with or without *N*-ethylmaleimide (NEM) (10 mM) in astrocytes and neurons. (*C*) Complex I subunits, excised from complex I-containing bands from a blue native gels, were rated according to their signal intensities. The arrow indicates the most easily observed complex I subunit (NDUFS1) present both in free and in bound (supercomplexes) complex I fractions in neurons and astrocytes. (*D*) NDUFS1 protein abundance in neurons and astrocytes, as assessed by BNGE either followed by direct electroblotting [also with complex III-UQCRC2 plus complex IV–MT-CO1 (mitochondrially encoded cytochrome C oxidase I) subunits] or by second-dimension SDS/PAGE immunoblotting followed by densitometric band intensity quantification. Coomassie-stained proteins from the BNGE were used as loading control. CIII, complex III subunit UQCRC2; CIV, complex IV subunit MT-CO1. Data are the mean values ± SEM from $n = 3$–4 independent culture preparations (Student's *t* test). $^*P < 0.05$.

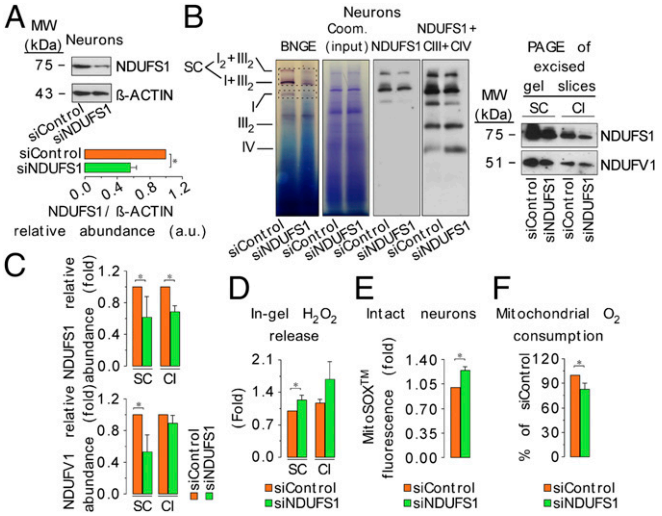

Fig. 4. NDUFS1 knockdown in neurons disassembles complex I from supercomplexes increasing ROS and impairing mitochondrial respiration. (*A*) Neurons were transfected with a siRNA against NDUFS1 (or a control siRNA), and 3 d after, NDUFS1 protein abundance was analyzed by Western blotting in the whole-cell extracts, followed by densitometric band quantification. β-Actin was used as loading control. (*B*) Digitonin-solubilized isolated mitochondria from NDUFS1–knocked-down neurons were subjected to BNGE followed by in-gel complex I activity assay, and direct electroblotting against complex I subunit NDUFS1, and complex III (UQCRC2) plus complex IV (MT-CO1). Bands corresponding to supercomplexes (SC) and free complex I (CI) were excised from the blue native gels, and subjected to second-dimension SDS/PAGE immunoblotting against NDUFS1 and NADH:ubiquinone oxidoreductase core subunit V1 (NDUFV1) NADH:ubiquinone oxidoreductase core subunit V1 (NDUFV1). NDUFV1 abundance was assessed to distinguish between expression or stability of complex I. Coomassie-stained proteins from the BNGE were used as loading control. (*C*) Densitometric quantification analyses of the NDUFS1 and NDUFV1 band intensities shown in *B*. (*D*) In-gel H_2O_2 production in the excised SC and CI bands from the BNGE of digitonin-solubilized isolated mitochondria from control and NDUFS1–knocked-down neurons. H_2O_2 production values were normalized by the NADH dehydrogenase-activity band intensity obtained in the BNGE. (*E*) Mitochondrial ROS assessed using the MitoSox assay in intact cells by flow cytometry. (*F*) Rate of pyruvate/malate (5 mM each; 1 mM ADP)-driven mitochondrial oxygen consumption in isolated mitochondria from neurons. CIII, complex III subunit UQCRC2; CIV, complex IV subunit MT-CO1. Data are the mean values ± SEM from n = 3–4 independent culture preparations (Student's t test). *$P < 0.05$.

I is one-third (~33%) of total complex I in astrocytes, but only ~5% in neurons. Given that deactive complex I preferentially transfers electrons to O_2 instead of to ubiquinone (30, 31), our results suggest that the high proportion of deactive complex I in astrocytes may contribute to the higher mitochondrial ROS production of these cells.

Modulation of Complex I Assembly into Supercomplexes Alters ROS Production and Respiration in Neurons and Astrocytes. To see whether ROS production and respiration are affected by the proportion of complex I incorporated into supercomplexes, we first assessed the relative abundance of complex I subunits in complex I-containing bands from the blue native gel. The majority of complex I subunits were asymmetrically distributed, both in astrocytes and in neurons (Fig. 3*C*). This is consistent with recent work showing different states of subcomplex I aggregates in aging (32). Interestingly, we observed that the only complex I subunit that was distributed equally in both cell types was NADH:ubiquinone oxidoreductase core subunit S1 (NDUFS1) (Fig. 3*C*), which harbors three out of the eight Fe–S clusters of complex I (33). Given its essential role in electron transfer, we next assessed the NDUFS1 protein abundance. NDUFS1 protein abundance was higher in neurons than in astrocytes, as judged by BNGE followed by immunoblotting directly, or after second-dimension SDS/PAGE (Fig. 3*D*). We found that NDUFS1 knockdown in neurons (Fig. 4*A*) diminished free and supercomplex-assembled complex I abundance (Fig. 4 *B* and *C*). Consistent with this, ROS production increased in free complex I and in complex I-containing supercomplexes bands excised from the blue native gel (Fig. 4*D*) and in the intact NDUFS1-silenced neurons (Fig. 4*E*). These effects impaired the electron transfer efficiency through the mitochondrial respiratory chain, as judged by the decreased pyruvate/malate-driven O_2 consumption (state 3) in isolated mitochondria (Fig. 4*F*). Conversely, NDUFS1 overexpression in astrocytes (Fig. 5*A*) increased free complex I and promoted its assembly into supercomplexes (Fig. 5 *B* and *C*). Consistent with this, ROS production by free complex I and complex I-containing supercomplexes excised from the blue native gel decreased (Fig. 5*D*), as did ROS production in the intact NDUFS1-overexpressing astrocytes (Fig. 5*E*). This was not associated with an increase in pyruvate/malate-driven O_2 consumption (state 3) (Fig. 5*F*), which is consistent with the low abundance of complex III in astrocytes limiting electron transfer to O_2 (Fig. 1*B*). Thus, modulation of complex I assembly into supercomplexes affects mitochondrial O_2 consumption and ROS production.

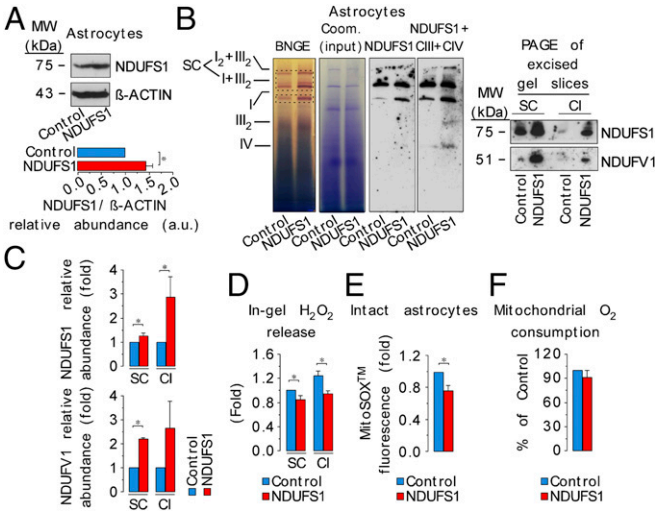

Fig. 5. Overexpression of NDUFS1 in astrocytes assembles complex I in supercomplexes and decreases ROS production. (*A*) Astrocytes were transfected with the full-length NDUFS1 cDNA (or control plasmid), and 1 d after, NDUFS1 protein abundance was analyzed by Western blotting in the whole-cell extracts, followed by densitometric band quantification. β-Actin was used as loading control. (*B*) Digitonin-solubilized isolated mitochondria from NDUFS1-overexpressing astrocytes were subjected to BNGE followed by in-gel complex I activity assay, and direct electroblotting against complex I subunit NDUFS1, and complex III (UQCRC2) plus complex IV (MT-CO1). Bands corresponding to supercomplexes (SC) and free complex I (CI) were excised from the blue native gel, and subjected to second-dimension SDS/PAGE immunoblotting against NDUFS1 and NDUFV1. Coomassie-stained proteins from the BNGE were used as loading control. (*C*) Densitometric quantification analyses of the NDUFS1 and NDUFV1 band intensities shown in *B*. (*D*) In-gel H_2O_2 production in the excised SC and CI bands from the BNGE of digitonin-solubilized isolated mitochondria from control and NDUFS1-overexpressing astrocytes. H_2O_2 production values were normalized by the NADH dehydrogenase-activity band intensity obtained in the BNGE. (*E*) Mitochondrial ROS as assessed using the MitoSox assay in intact cells by flow cytometry. (*F*) Rate of pyruvate/malate (5 mM each; 1 mM ADP)-driven mitochondrial oxygen consumption in isolated mitochondria from astrocytes. CIII, complex III subunit UQCRC2; CIV, complex IV subunit MT-CO1. Data are the mean values ± SEM from n = 3–4 independent culture preparations (Student's t test). *$P < 0.05$.

Discussion

Here, we report that neurons and astrocytes organize their mitochondrial respiratory chains differently, with altered proportions of complex I free or present in supercomplexes. In astrocytes, less complex I is assembled into supercomplexes, leaving more free complex I. In contrast, in neurons, more complex I is assembled into supercomplexes. These differences correlate with changes in ROS production and respiration, with the more free complex I segregating with elevated ROS production. Furthermore, these rates of mitochondrial ROS formation are altered by reorganizing the mitochondrial respiratory chain in response to up-modulation and down-modulation of NDUFS1 levels. Interestingly, the rate of ROS formation inversely correlated with electron transfer efficiency in neurons, with NDUFS1 knockdown impairing mitochondrial O_2 consumption but increasing ROS. In contrast, NDUFS1 overexpression in astrocytes decreased ROS, although it did not increase mitochondrial O_2 consumption. This effect on free complex I abundance can be explained by the reduced abundance of complex III in astrocytes that limits the amount of complex I that can be sequestered into supercomplexes.

The lack of effect of ADP at stimulating pyruvate/malate O_2 consumption in astrocyte mitochondria is in good agreement with the high deactive complex I proportion, and the low complex III abundance, found in these cells. Thus, NADH-derived electrons are inefficiently transferred to ubiquinone by deactive complex I (30, 31), and subsequently to complex IV due to the low proportion of complex III in astrocytes. Moreover, given the low complex III abundance in astrocytes, it would be reasonable to speculate that ubiquinone pool would be favored toward its reduced status, a factor known to cause complex I deactivation (34). Whether a positive loop of complex I deactivation, which is promoted by ROS (34), takes place in astrocytes is a tempting possibility that remains to be explored.

Our results may help explain the different redox and bioenergetic features of neurons and astrocytes. Thus, the greater proportion of complex I assembled into supercomplexes in neurons may contribute to the higher respiration rate of neurons compared with astrocytes. This is consistent with the dependence of neurons on oxidative phosphorylation for neurotransmission and survival (17–19). In contrast, the smaller proportion of complex I that is assembled into supercomplexes in astrocytes may contribute to their lower respiration rate and is consistent with their more glycolytic metabolism (17–22). A further intriguing aspect is that the large difference in mitochondrial ROS production between neurons and astrocytes correlates with the amount of free complex I. This may explain why astrocytes produce more ROS than neurons, and hence are equipped with a robust redox antioxidant system (35, 36). Indeed, astrocytes express functionally active Nrf2 (11), a transcription factor that is activated by ROS (37) and governs expression of a range of antioxidant genes that protect both astrocytes and their neighboring neurons (38).

In conclusion, the extent of assembly of complex I into supercomplexes is different between neurons and astrocytes, and contributes to some of the differences in mitochondrial metabolism and ROS generation between these cells. However, the functional and mechanistic role of supercomplexes is currently unclear and disputed (39). In future work, it will be important to determine whether the differences in respiration and ROS between neurons and astrocytes are due to the properties of the supercomplexes themselves (40), or whether the balance between the relative levels of complexes I and III is more critical. Furthermore, it will be very interesting to explore whether changes in complex I incorporation into supercomplexes and/or its balance with complex III contribute to excessive ROS associated in pathological situations, such as in the dopaminergic neuronal death in Parkinson's disease (41–43). If so, interventions aimed at maintaining complex I stability would be a promising therapeutic approach against this, and other neurodegenerative diseases.

Materials and Methods

Ethical Use of Animals. Wistar rats and C57BL/6 mice were bred at the Animal Experimentation Unit of the University of Salamanca. All protocols were approved by the Bioethics Committee of the University of Salamanca in accordance with the Spanish legislation (law 6/2013).

Primary Cell Cultures. Primary cultures of Wistar rat or C57BL/6 mouse cortical neurons and astrocytes were prepared from embryonic day 15.5–16.5 (neurons) or postnatal 0–24 h (astrocytes), as described previously (44) (*SI Materials and Methods*).

Mitochondria Isolation and Solubilization. Mitochondria were isolated according to a previously published protocol (24) and solubilized with digitonin at 4 g/g (5 min in ice) (*SI Materials and Methods*).

Mitochondrial Respiration. To measure the state 3 oxygen consumption rates, we used a Clark-type electrode (Rank Brothers). Neuronal and astrocytic cells were recollected by trypsinization and mitochondria were immediately obtained. Freshly isolated mitochondria (100 μg) were suspended in the respiration medium (125 mM KCl, 2 mM KH_2PO_4, 1 mM $MgCl_2$, 0.5 mg/mL BSA, 10 mM Hepes, pH 7.4). Oxygen consumption was determined after the addition of 5 mM pyruvate plus 5 mM malate, or 5 mM succinate (state 2), followed by the addition of 1 mM ADP (state 3).

ROS Determination. Mitochondrial ROS was detected using the fluorescent probe MitoSox (Life Technologies) and MitoB probe (*SI Materials and Methods*). For H_2O_2 assessments, AmplexRed (Life Technologies) was used (*SI Materials and Methods*). H_2O_2 measured directly form blue native gel slices were performed in the presence of 20 μM NADH and 40 U/mL SOD (*SI Materials and Methods*).

Mitochondrial Membrane Potential. The mitochondrial membrane potential ($\Delta\psi_m$) was assessed using the probe DiIC1 (5) (Life Technologies) (50 nM) by flow cytometry (*SI Materials and Methods*).

Activity of Mitochondrial Complexes. Cells were collected and suspended in phosphate buffer (PB: 0.1 M KH2PO4 pH 7.0). After three cycles of freeze/thawing, to ensure cellular disruption, complex I, complex II, complex II–III, complex IV, and citrate synthase activities were determined spectrophotometrically as indicated in *SI Materials and Methods*.

BNGE. For the assessment of complex I organization, digitonin-solubilized mitochondria (10–50 μg) were loaded in NativePAGE Novex 3–12% (vol/vol) gels (Life Technologies). After electrophoresis, in-gel NADH dehydrogenase activity was evaluated (45). After identification of individual complex I and complex I-containing supercomplexes bands according to the NADH dehydrogenase activity, either a direct electrotransfer or a second-dimension SDS/PAGE were performed to identify some subunits of the mitochondrial complexes. Thus, individual complex I or complex I-containing supercomplexes bands were excised from the gel and denatured in 1% SDS (containing 1% β-mercaptoethanol) during 1 h. The proteins contained in the gel slices were separated electrophoretically, followed by Western blotting against NDUFS1- or NDUFV1-specific antibodies. Coomassie staining of BNGE gels was performed, as an indicator of loaded protein, during 15 min followed by different steps of destaining with 10% (vol/vol) acetic acid plus 20% (vol/vol) methanol. Direct transfer of BNGE was performed after soaking the gels for 20 min (4 °C) in carbonate buffer (10 mM $NaHCO_3$, 3 mM $Na_2CO_3{\cdot}10H_2O$, pH 9.5–10). Proteins transfer to nitrocellulose membranes was carried out at 300 mA, 60 V, 1 h at 4 °C in carbonate buffer.

Electroelution of Proteins. Following BNGE and in-gel NADH dehydrogenase activity, individual and complex I-containing supercomplexes bands were excised, and the proteins electroeluted. To electroelute proteins, gel slices were placed in an electrodialysis membrane (Dialysis Tubing-Visking; Medicall International), and an electric field was applied during 4 h at 100 V. The samples containing the electroeluted proteins were collected, and the complex I-specific activity was determined.

Mass Spectrometry. Mass spectrometry analysis was carried out in the blue native gel slices excised from the individual complex I, complex I-containing supercomplexes, and in the interbands, at the Medical Research Council Mitochondrial Biology Unit (Cambridge, UK) as described in *SI Materials and Methods*.

Protein Determinations. Protein samples were quantified by the BCA protein assay kit (Thermo) following the manufacturer's instructions, using BSA as a standard.

Statistical Analysis. All measurements were carried out at least in three different culture preparations or animals, and the results were expressed as the mean values ± SEM. For the comparisons between two groups of values, the statistical analysis of the results was performed by Student's *t* test. For multiple-values comparisons, we used one-way ANOVA followed by the Bonferroni test. The statistical analysis was performed using the SPSS software. In all cases, $P < 0.05$ was considered significant.

ACKNOWLEDGMENTS. We acknowledge Monica Carabias and Monica Resch for technical assistance; Noëlle Dufour, Charlène Joséphine, and Alexis Bemelmans for AAVs production; and Charlène Joséphine, Martine Guillermier, Diane Houitte, and Gwenaëlle Aurégan for stereotaxic injections of AAVs. J.P.B. is funded by the Ministry of Economy and Competitiveness (SAF2013-41177-R), Instituto de Salud Carlos III (RD12/0043/0021), European Union (EU) SP3-People-MC-ITN Programme (608381), EU BATCure Grant 666918, and NIH/National Institute on Drug Abuse Grant 1R21DA037678-01. A.A. is funded by Instituto de Salud Carlos III (PI12/00685 and RD12/0014/0007).

1. Magistretti PJ (2006) Neuron-glia metabolic coupling and plasticity. *J Exp Biol* 209(Pt 12): 2304–2311.
2. Allen NJ, Barres BA (2009) Neuroscience: Glia—more than just brain glue. *Nature* 457(7230):675–677.
3. Kimelberg HK, Nedergaard M (2010) Functions of astrocytes and their potential as therapeutic targets. *Neurotherapeutics* 7(4):338–353.
4. Perea G, Sur M, Araque A (2014) Neuron-glia networks: Integral gear of brain function. *Front Cell Neurosci* 8:378.
5. Parpura V, et al. (1994) Glutamate-mediated astrocyte-neuron signalling. *Nature* 369(6483):744–747.
6. Perea G, Navarrete M, Araque A (2009) Tripartite synapses: Astrocytes process and control synaptic information. *Trends Neurosci* 32(8):421–431.
7. Araque A, et al. (2014) Gliotransmitters travel in time and space. *Neuron* 81(4): 728–739.
8. Oliveira JF, Sardinha VM, Guerra-Gomes S, Araque A, Sousa N (2015) Do stars govern our actions? Astrocyte involvement in rodent behavior. *Trends Neurosci* 38(9): 535–549.
9. Schreiner B, et al. (2015) Astrocyte depletion impairs redox homeostasis and triggers neuronal loss in the adult CNS. *Cell Rep* 12(9):1377–1384.
10. Makar TK, et al. (1994) Vitamin E, ascorbate, glutathione, glutathione disulfide, and enzymes of glutathione metabolism in cultures of chick astrocytes and neurons: Evidence that astrocytes play an important role in antioxidative processes in the brain. *J Neurochem* 62(1):45–53.
11. Jimenez-Blasco D, Santofimia-Castaño P, Gonzalez A, Almeida A, Bolaños JP (2015) Astrocyte NMDA receptors' activity sustains neuronal survival through a Cdk5-Nrf2 pathway. *Cell Death Differ* 22(11):1877–1889.
12. Dringen R, Pfeiffer B, Hamprecht B (1999) Synthesis of the antioxidant glutathione in neurons: Supply by astrocytes of CysGly as precursor for neuronal glutathione. *J Neurosci* 19(2):562–569.
13. Bolaños JP, Heales SJR, Land JM, Clark JB (1995) Effect of peroxynitrite on the mitochondrial respiratory chain: Differential susceptibility of neurones and astrocytes in primary culture. *J Neurochem* 64(5):1965–1972.
14. Bolaños JP, et al. (1996) Nitric oxide-mediated mitochondrial damage: A potential neuroprotective role for glutathione. *Free Radic Biol Med* 21(7):995–1001.
15. Deighton RF, et al. (2014) Nrf2 target genes can be controlled by neuronal activity in the absence of Nrf2 and astrocytes. *Proc Natl Acad Sci USA* 111(18):E1818–E1820.
16. Baxter PS, et al. (2015) Synaptic NMDA receptor activity is coupled to the transcriptional control of the glutathione system. *Nat Commun* 6:6761.
17. Almeida A, Moncada S, Bolaños JP (2004) Nitric oxide switches on glycolysis through the AMP protein kinase and 6-phosphofructo-2-kinase pathway. *Nat Cell Biol* 6(1):45–51.
18. Almeida A, Almeida J, Bolaños JP, Moncada S (2001) Different responses of astrocytes and neurons to nitric oxide: The role of glycolytically generated ATP in astrocyte protection. *Proc Natl Acad Sci USA* 98(26):15294–15299.
19. Herrero-Mendez A, et al. (2009) The bioenergetic and antioxidant status of neurons is controlled by continuous degradation of a key glycolytic enzyme by APC/C-Cdh1. *Nat Cell Biol* 11(6):747–752.
20. Pellerin L, Magistretti PJ (1994) Glutamate uptake into astrocytes stimulates aerobic glycolysis: A mechanism coupling neuronal activity to glucose utilization. *Proc Natl Acad Sci USA* 91(22):10625–10629.
21. Bouzier-Sore AK, Voisin P, Canioni P, Magistretti PJ, Pellerin L (2003) Lactate is a preferential oxidative energy substrate over glucose for neurons in culture. *J Cereb Blood Flow Metab* 23(11):1298–1306.
22. Allaman I, Bélanger M, Magistretti PJ (2011) Astrocyte-neuron metabolic relationships: For better and for worse. *Trends Neurosci* 34(2):76–87.
23. Bianchi C, Genova ML, Parenti Castelli G, Lenaz G (2004) The mitochondrial respiratory chain is partially organized in a supercomplex assembly: Kinetic evidence using flux control analysis. *J Biol Chem* 279(35):36562–36569.
24. Acín-Pérez R, Fernández-Silva P, Peleato ML, Pérez-Martos A, Enriquez JA (2008) Respiratory active mitochondrial supercomplexes. *Mol Cell* 32(4):529–539.
25. Lapuente-Brun E, et al. (2013) Supercomplex assembly determines electron flux in the mitochondrial electron transport chain. *Science* 340(6140):1567–1570.
26. Kussmaul L, Hirst J (2006) The mechanism of superoxide production by NADH:ubiquinone oxidoreductase (complex I) from bovine heart mitochondria. *Proc Natl Acad Sci USA* 103(20):7607–7612.
27. Murphy MP (2009) How mitochondria produce reactive oxygen species. *Biochem J* 417(1):1–13.
28. Cochemé HM, et al. (2011) Measurement of H_2O_2 within living *Drosophila* during aging using a ratiometric mass spectrometry probe targeted to the mitochondrial matrix. *Cell Metab* 13(3):340–350.
29. Foo LC (2013) Purification of rat and mouse astrocytes by immunopanning. *Cold Spring Harb Protoc* 2013(5):421–432.
30. Babot M, et al. (2014) ND3, ND1 and 39kDa subunits are more exposed in the deactive form of bovine mitochondrial complex I. *Biochim Biophys Acta* 1837(6): 929–939.
31. Roberts PG, Hirst J (2012) The deactive form of respiratory complex I from mammalian mitochondria is a Na^+/H^+ antiporter. *J Biol Chem* 287(41):34743–34751.
32. Miwa S, et al. (2014) Low abundance of the matrix arm of complex I in mitochondria predicts longevity in mice. *Nat Commun* 5:3837.
33. Janssen RJ, Nijtmans LG, van den Heuvel LP, Smeitink JA (2006) Mitochondrial complex I: Structure, function and pathology. *J Inherit Metab Dis* 29(4):499–515.
34. Dröse S, Stepanova A, Galkin A (2016) Ischemic A/D transition of mitochondrial complex I and its role in ROS generation. *Biochim Biophys Acta* 1857(7):946–957.
35. Diaz-Hernandez JI, Almeida A, Delgado-Esteban M, Fernandez E, Bolaños JP (2005) Knockdown of glutamate-cysteine ligase by small hairpin RNA reveals that both catalytic and modulatory subunits are essential for the survival of primary neurons. *J Biol Chem* 280(47):38992–39001.
36. Fernandez-Fernandez S, Almeida A, Bolaños JP (2012) Antioxidant and bioenergetic coupling between neurons and astrocytes. *Biochem J* 443(1):3–11.
37. Tebay LE, et al. (2015) Mechanisms of activation of the transcription factor Nrf2 by redox stressors, nutrient cues, and energy status and the pathways through which it attenuates degenerative disease. *Free Radic Biol Med* 88(Pt B):108–146.
38. Johnson DA, Johnson JA (2015) Nrf2—a therapeutic target for the treatment of neurodegenerative diseases. *Free Radic Biol Med* 88(Pt B):253–267.
39. Blaza JN, Serreli R, Jones AJ, Mohammed K, Hirst J (2014) Kinetic evidence against partitioning of the ubiquinone pool and the catalytic relevance of respiratory-chain supercomplexes. *Proc Natl Acad Sci USA* 111(44):15735–15740.
40. Maranzana E, Barbero G, Falasca AI, Lenaz G, Genova ML (2013) Mitochondrial respiratory supercomplex association limits production of reactive oxygen species from complex I. *Antioxid Redox Signal* 19(13):1469–1480.
41. Perry TL, Godin DV, Hansen S (1982) Parkinson's disease: A disorder due to nigral glutathione deficiency? *Neurosci Lett* 33(3):305–310.
42. Schapira AH, et al. (1989) Mitochondrial complex I deficiency in Parkinson's disease. *Lancet* 1(8649):1269.
43. Schapira AH (2012) Mitochondrial diseases. *Lancet* 379(9828):1825–1834.
44. Requejo-Aguilar R, et al. (2014) PINK1 deficiency sustains cell proliferation by reprogramming glucose metabolism through HIF1. *Nat Commun* 5:4514.
45. Diaz F, Barrientos A, Fontanesi F (2009) Evaluation of the mitochondrial respiratory chain and oxidative phosphorylation system using blue native gel electrophoresis. *Curr Protoc Hum Genet* Chapter 19:Unit19.4.
46. Subbalakshmi GY, Murthy CR (1985) Isolation of astrocytes, neurons, and synaptosomes of rat brain cortex: Distribution of enzymes of glutamate metabolism. *Neurochem Res* 10(2):239–250.
47. Ragan CI, Wilson MT, Darley-Usmar VM, Lowe PN (1987) Subfractionation of mitochondria and isolation of the proteins of oxidative phosphorylation. *Mitochondria: A Practical Approach*, eds Darley-Usmar VM, Rickwood D, Wilson MT (IRL, London), pp 79–112.
48. King TE (1967) Preparation of succinate cytochrome *c* reductase and the cytochrome *b*-c_1 particle, and reconstitution of succinate cytochrome *c* reductase. *Methods Enzymol* 10:216–225.
49. Wharton DC, Tzagoloff A (1967) Cytochrome oxidase from beef heart mitochondria. *Methods Enzymol* 10:245–250.
50. Shepherd D, Garland PB (1969) The kinetic properties of citrate synthase from rat liver mitochondria. *Biochem J* 114(3):597–610.
51. Starkov AA (2010) Measurement of mitochondrial ROS production. *Methods Mol Biol* 648:245–255.
52. Olsen C, Rustad A, Fonnum F, Paulsen RE, Hassel B (1999) 3-Nitropropionic acid: An astrocyte-sparing neurotoxin in vitro. *Brain Res* 850(1-2):144–149.